Scientific Research Publishing

Energy and Power Engineering, 2024, 16, 373-393
https://www.scirp.org/journal/epe
ISSN Online: 1947-3818
ISSN Print: 1949-243X

Design and Optimized Control of a Photovoltaic/Battery-Powered Cathodic Protection System

Amal A. Hassan*, Hanaa M. Farghally, Abd El-Shafy A. Nafeh, Ninet M. Ahmed, Faten H. Fahmy

Electronics Research Institute, Cairo, Egypt
Email: *amal.elramly@eri.sci.eg

How to cite this paper: Hassan, A.A., Farghally, H.M., Nafeh, A.E.-S.A., Ahmed, N.M. and Fahmy F.H. (2024) Design and Optimized Control of a Photovoltaic/Battery-Powered Cathodic Protection System. *Energy and Power Engineering*, **16**, 373-393.
https://doi.org/10.4236/epe.2024.1612019

Received: November 3, 2024
Accepted: December 10, 2024
Published: December 13, 2024

Abstract

Metallic pipeline corrosion poses a significant challenge in the petrochemical industry. In this study, the design and control of a stand-alone photovoltaic (PV)-powered cathodic protection (CP) system based on the impressed current method were investigated. The proposed CP system was applied to a 250 km long steel-buried pipeline in the Sharm El-Sheikh region of Egypt. The system design involved the numerical modeling of the anode bed for the impressed current CP (ICCP) system and the sizing of the DC power source, including the PV array and battery bank. The system was designed and controlled to deliver a constant and continuous anode current to protect the underground pipeline from corrosion during daylight and nighttime. A maximum power point tracking (MPPT) algorithm based on the fractional open-circuit voltage (FOCV) technique was implemented to maximize power extraction from the PV array. Additionally, a proportional-integral (PI) controller was optimized and employed to achieve MPPT, while another PI controller managed the anode current of the CP system. Safe charging and discharging of the system's battery are ensured via an ON-OFF controller. The parameters of the PI controllers were optimized using the particle swarm optimization (PSO) technique. Simulation results demonstrated that the proposed CP system achieved the required protection objectives successfully.

Keywords

Photovoltaic, Cathodic Protection, MPPT, PI Controller, PSO Optimization

1. Introduction

Corrosion poses a significant challenge for the petrochemical and petroleum industries. It can severely impact the integrity and lifespan of refinery equipment if

not adequately mitigated. Corrosion monitoring and prevention require ongoing inspection, maintenance, and mitigation efforts. However, some corrosion mechanisms occur underground or inside dense equipment, making visual inspection impractical [1]. Cathodic protection (CP) is a corrosion control and prevention technique that can be applied to various structures in different environments, including buried and immersed metallic structures. CP is an electrochemical corrosion control technique in which an oxidation reaction occurs at the anode of a galvanic cell and prevents corrosion at the cathode of the same cell. CP works by preventing anodic reactions of metal corrosion on the structure being protected, thereby preventing metal dissolution [2] [3]. This goal is accomplished by allowing anodic reactions on specially designed and mounted anodes. Two ways could be utilized: an impressed current CP (ICCP) method or a sacrificial anode (galvanic action) CP. There is no power supply to feed the system in the sacrificial anode. At the same time, the ICCP system requires an energy supply to impress the current through the anode. If available, this power may be obtained from the utility grids, and then a rectifier can feed the CP-DC load. Another alternative is to use renewable energy-based standalone DC power sources [4].

ICCP is a method utilized to manage corrosion in steel structures. It is extensively applied across the oil and gas, marine and port sectors and in offshore wind farms, safeguarding assets like underground or buried pipelines from natural degradation. Consequently, it enhances safety, maintains process continuity, and protects the environment by minimizing the chances of leakages from oil and gas pipelines and infrastructure [3] [5]. ICCP is typically implemented on larger structures where galvanic anodes cannot deliver the required current for complete protection. In ICCP systems, anodes are linked to a DC power supply called a CP rectifier. Various materials such as silicon, cast iron, graphite, mixed metal oxide, platinum, and niobium-coated wire are used as anodes in ICCP systems. ICCP can reduce the rate of corrosion according to the applied current. Specific solutions can extend the lifespan of an item by nearly eliminating corrosion.

Several previous studies have examined the numerical modeling and design of corrosion protection systems for pipeline networks [6]-[8]. Mustafa Al-Refai [9] developed a numerical approach for calculating the appropriate design of an ICCP system. The model allows for simulation and optimization of ICCP design parameters such as cathode placement and required electrical characteristics. Mohamed Saif *et al.* [10] [11] presented work on implementing and analyzing a CP station for pipeline corrosion control. Their studies involved developing mathematical models to simulate CP station operation and analyze factors like voltage gradients and protection current requirements along the pipeline. Wind, solar, tidal, and hydroelectric power facilities are some of the technical options used as the power source for the ICCP [2] [3]. Solar energy is the best option of all renewable energy sources that may be utilized as a DC power source [12]. In previous research, researchers have concentrated on three major areas [4] to improve the efficiency of PV systems: creating solar irradiance tracking systems, implementing efficient

power converters, and establishing maximum power point tracking (MPPT) methods [13]. Javidan *et al.* [13] [14] proposed a solar PV system for CP of underground pipelines. They use a buck-boost converter for battery charging and a buck converter at PV system terminals. In [15], Mourad *et al.* also proposed two controllers for DC-DC converters: a buck converter to track the MPPT of PV and a buck-boost converter between battery and load. In [16], Laoun *et al.* proposed designing a CP system supplied by solar PV arrays. Golina *et al.* [17] provided a design and sizing of a PV-based CP system.

B. Sada *et al.* [18] designed PID and fuzzy logic controllers (FLC) to regulate ICCP system output variables like voltage and current. Javadi *et al.* [19] presented an MPPT controller for optimizing output from a photovoltaic array powering an ICCP system. The study implemented both perturbation and observation (P&O) and incremental conductance (IC) MPPT algorithms to dynamically adjust the buck converter based on solar irradiance levels throughout the day. Additionally, authors in [20] developed an FLC method to compensate for environmental fluctuations and dynamic changes along an Iraq-Turkey crude oil pipeline protected by ICCP. The FLC was tested in two application regions and showed an improved ability to maintain protective voltages versus fluctuations compared to a conventional ICCP controller.

Despite extensive global studies, prior studies lack comprehensive designs that address the real-world challenges of stand-alone PV-powered ICCP systems, such as adapting to varying solar conditions. Only some studies [18] [20] address the challenge of optimizing multiple controllers in ICCP systems powered by renewable sources. While some attempt fuzzy logic or PID approaches, they do not combine these with advanced optimization methods like PSO for improved system stability and efficiency. Moreover, minimal research focuses on the specific corrosion and environmental challenges in regions like Egypt, where pipelines span significant distances under harsh conditions and solar energy is abundant.

This paper presents the design and control strategy for a standalone PV-powered CP system using the impressed current method for a 250 km long steel pipeline in Sharm El-Sheik, Egypt. The system design includes the numerical design of the anode bed of the ICCP system and the sizing of the standalone PV system. The CS system control is developed to supply a continuous constant anode current for pipeline protection against corrosion. The fractional open-circuit voltage (FOCV) MPPT algorithm helps to maximize the PV array power extraction during daylight. Three controllers are developed: the first for the PV array's MPPT, the second for regulating the CP system's anode current, and the third for charging and discharging the system battery. The parameters of the PI controllers are optimized using the particle swarm optimization (PSO) technique.

The main contributions of the paper are:

- This study develops a detailed design for a stand-alone PV-powered ICCP system, including optimized PV array sizing, battery storage, and anode bed for a 250 km buried steel pipeline.

- Implementing FOCV MPPT for enhanced PV efficiency.
- Regulating anode current to ensure adequate corrosion protection.
- Managing battery charging and discharging for continuous operation under varying solar conditions.
- The study improves system reliability and performance under environmental and operational dynamics by integrating advanced control algorithms and optimization techniques.
- This research addresses the unique needs of Egyptian infrastructure, reducing dependence on grid power and providing a sustainable, renewable energy-based solution tailored to regional challenges.

The paper is organized as follows: Section 2 outlines the design of the ICCP system, including the calculation of the necessary total anode resistance. Additionally, this section addresses the design of the PV-battery power source to meet the demands of the ICCP load. Section 3 focuses on modeling the PV, battery, and DC-DC converter components and the control strategies for MPPT and power management. Section 4 presents the findings from simulating the proposed ICCP power system under various operating scenarios. Lastly, conclusions are drawn concerning the technical viability and benefits of the renewable PV-battery solution for self-sufficient ICCP applications.

2. Cathodic Protection System Design

Figure 1 shows the proposed photovoltaic/battery-powered CP system block diagram. The key components include a PV array, boost DC-DC converter, battery bank, battery regulator, buck-boost DC-DC converter, and the protected pipeline serving as the anode bed load. Additionally, there are three controllers for the converters of the proposed system to properly manage and control the power flow and control within the system. The design, functionality, and control of the system components will be clarified in detail later in this paper.

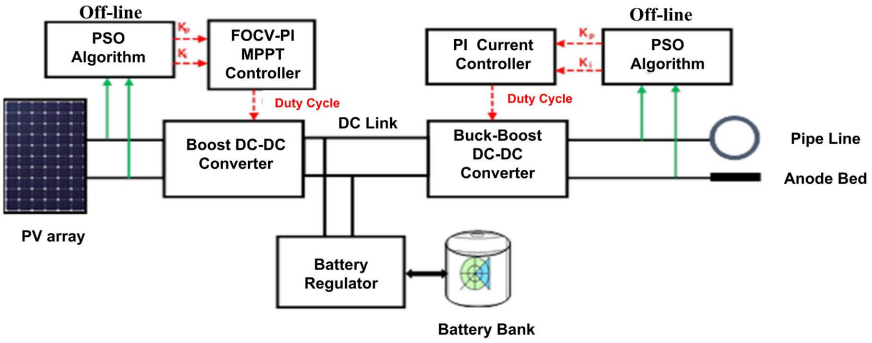

Figure 1. Block diagram of the PV/battery-powered CP system.

2.1. Sizing of the Proposed ICCP System

In this work, a CP system with a lifetime of 30 years is designed to protect the pipeline of 250 km length and 0.914 m diameter used for natural gas transfer in

Sharm El-Sheik City, located in the South Sinai of Egypt. The pipeline structure's physical dimensions, such as length and diameter, are essential in designing a CP system. These parameters are used to calculate the total surface area to be protected and consequently will affect the required total current. Table 1 summarizes the pipeline characteristics and dimensions considered. Different design parameter calculations will be discussed in the following sections.

Table 1. Pipeline characteristics and dimensions.

Length (m)	250,000
Diameter (m)	0.914
Coating efficiency (η_c)	98%
Area (m^2)	717853.9
A_u (m^2)	14,363

Proper sizing of the anode network is crucial so that the installed CP system can generate sufficient current to meet the demand calculated from the pipeline parameters and prevent external corrosion from occurring over the design life. The initial step in sizing involves calculating the surface area of the pipeline. The subsequent equation can be utilized to find the pipeline's total external surface area (A) in a desert environment [11].

$$A = \pi DL \tag{1}$$

This equation is relevant for cylindrical forms as the distribution pipelines are determined by: L, which signifies the length of the pipeline, and D, the pipeline's diameter. After that, the unprotected surface area, A_u, that requires protection is estimated. This accounts for the coating efficiency (η_c), typically around 98% for modern coatings and can be calculated as follows [8] [11]:

$$A_u = (1-\eta_c) \times A \tag{2}$$

The total protective current demand is then calculated using the unprotected area and theoretical current density needed to prevent corrosion. This current density value depends on the type of soil and its chemical characteristics. The total current required to prevent corrosion (I_{cc}) is calculated depending on the following formula [8] [11]:

$$I_{cc} = J_c \times A_u \tag{3}$$

J_c is the minimum current density required to prevent corrosion of the pipeline. The value of J_c is typically around 0.0004 A/m^2 [21]. To effectively protect buried pipelines, a continuous source of electrical current must be supplied. The amount of current needed is based on the surface characteristics of the metal, surrounding soil chemistry, and exposed area. For CP systems in desert environments, aluminum is commonly used for the design of the impressed current anodes due to its availability and ease of construction. The required number of anodes, N_A, to provide the total protective current, I_{cc}, is determined. This involves calculating N_A

based on I_{cc} and the anode current, I_A, that each anode can provide according to its material and design specifications [8] [11]:

$$N_A = \frac{I_{cc}}{I_A} \tag{4}$$

The next step in sizing of the ICCP system is to determine the total resistance of the ICCP circuit, which can be calculated using the following formula:

$$R_T = R_{pl} + R_{ta} + R_{gb} + R_c \tag{5}$$

where, R_{Pl} is the pipeline metallic structure resistance, R_{ta} is the total anode resistance, R_{gb} is the ground-bed resistance, and R_c is the total resistance of electrical cables.

The metallic structure of the pipeline distribution network's resistance (R_{pl}) can be calculated using the formula [21]:

$$R_{pl} = \frac{3.3}{4w} \times 10^{-3} \times L \tag{6}$$

where, w is the one-meter length mass of the pipeline. For desert environment, the value of w equals 40.24 kg/m [21].

The ground-bed resistance, R_{gb}, has a fixed resistance of 1.5 Ω, for desert environment [21]. While the resistance of a single anode (R_a) can be calculated using the following equation [21]:

$$R_a = \frac{\rho}{2 \times \pi \times L_A} \times \left[\ln\left(\frac{8 \times l_A}{D_A} \right) - 1 \right] \tag{7}$$

where ρ is the resistivity of the anode material (= 50 Ω·cm), l_A is the length of the anode (= 0.5 m), D_A is the diameter of the anode (= 0.025 m). Assuming all anodes have the same value of R_a, then the total resistance of multiple anodes connected in parallel (R_{ta}) becomes equal to R_a/N_A. Where N_A is the number of total anodes connected in parallel.

The voltage (V_R) needed from the DC power supply to provide the ICCP system with electrical current for enhanced corrosion protection is determined as [21]:

$$V_R = I_R \times R_T + V_{RB} \tag{8}$$

Table 2 summarizes the required CP daily load data needed to achieve the CP process of the considered pipeline.

Table 2. Electrical requirements of the ICCP system.

I_R (A)	5.745
V_R (V)	44.650
P_R (W)	256.5179
E_R (Wh)	6156.431

2.2. Standalone PV System Sizing

Standalone PV systems are designed to operate independently from the electricity

grid and are typically designed to supply power to specific DC and/or AC loads. There are various kinds of standalone PV systems; the most basic is the direct-coupled system, where the DC output from a PV array connects directly to a DC load, meaning that the load functions only during daylight hours. The system must generate electricity even at night in specific standalone PV configurations. Consequently, storage batteries are incorporated into the system. Batteries are primarily utilized to store surplus PV energy and later deliver it to the load when insufficient. Various battery types can be employed, including lead-acid, nickel-cadmium, and lithium-ion. In this analysis, a standalone PV system, which consists of a PV array and a lead-acid storage battery, is utilized to continuously provide power to the electrical load of the proposed CP system at all hours, both day and night. Thus, to achieve this, it is essential to accurately size the PV array and battery bank. The chosen PV modules are mono-crystalline silicon with a nominal MPP output of 220 W_P, a nominal MPP voltage of 29.21 V, and a nominal MPP current of 7.5317 A at standard test conditions (*i.e.*, 1000 W/m^2 and 25˚C). Additionally, the selected battery units are lead-acid batteries with a capacity of 100 Ah and 12 V each. The detailed system sizing will be presented in the following sections.

2.2.1. PV Array Sizing

The number of PV modules that should be connected in series, N_S, can be estimated in terms of the designed system DC link voltage, V_{DC} = 48 V, and the value of V_M by using the following equation [22]:

$$N_S = \frac{V_{DC}}{V_M} \tag{9}$$

But, to be compatible with the requirements of the input and output voltages of the utilized boost converter of **Figure 1**, it is necessary to refer the value of the system DC link voltage to the input side of the boost converter using nominal duty cycle of 0.5. Thus, the utilized value of V_{DC} at the PV side becomes 24 V. Consequently, the value of N_S becomes 1 module.

To determine the number of parallel strings of the utilized PV array [23], the load data obtained in **Table 2** is used to determine the required total nominal MPP current, I_p, of the PV array, by:

$$I_p = \frac{24 \times I_l}{PSH} \tag{10}$$

The *PSH* indicated in the previous equation is the selected site's peak solar hours, defined as the daily number of hours of standard radiation (*i.e.*, 1 kW/m^2) that produces the same daily irradiation. Thus, the value of the PSH of the selected site equals the numerical value of the daily irradiation in kW/m^2/day of the considered site. As the annual average daily irradiation of the selected site is 5.4 kWh/m^2/day [24], the PSH of the considered site becomes 5.4 h. Also, since the average daily load current demanded for the CP system is estimated to be $I_l = I_{cc} = I_R$ = 5.745 A, the value of I_p will be 25.5333 A. Consequently, the required number

of parallel strings of the utilized PV array (N_P) can be given by:

$$N_p = \frac{I_p}{I_M} \tag{11}$$

Thus, four strings are used to supply the required energy for the ICCP load, and therefore the total required PV power becomes 880 Wp.

2.2.2. Battery Bank Sizing

The storage battery capacity in Wh can be calculated using the following equation [22]:

$$\text{Battery Capacity} = \frac{N_C \times E_L}{DOD \times \eta_{out}} \tag{12}$$

where, N_C is the number of continuous cloudy days in the selected region (≈3 days), E_L is the load energy in Wh, DOD is the maximum permissible depth of discharge of the battery (≈0.8) and η_{out} is combined efficiency of the battery, battery regulator, and the buck-boost converter (≈0.765).

As, the required DC link voltage is 48 V, Equation (12) will yield a 628.7 Ah total storage capacity. Consequently, the utilized battery bank is configured as 4 battery units in series and 7 battery strings in parallel to yield a total storage capacity for the designed CP system of 700 Ah.

3. System Modeling, Simulation and Control

The configuration of the proposed PV/battery-powered CP system utilized in this work is illustrated previously in **Figure 1**. As indicated the PV array is used for supplying the electrical load of the CP system with the converted solar PV energy. The boost DC-DC converter is used to extract the maximum obtainable power of the PV array and transfer it to the CP load and also to transfer the excess PV power to charge the battery bank whenever needed. At the same time, this converter is used to step-up the PV array voltage to the suitable value needed for charging or discharging the system battery. The battery regulator is used to safely charge or discharge the battery bank whenever needed. Whereas, the buck-boost converter is used to supply the CP load with the suitable current needed to perform the CP process of the pipeline. In addition, it's necessary to note that there is a dump load connected at the output terminals of the boost DC-DC converter, which is properly designed to dissipate the excess PV energy in case of full charging of the system battery. This dump load can be switched ON or OFF by utilizing a switch which is controlled by an ON/OFF control signal. The PV array output current is expressed as [25]:

$$I_{pv} = N_p I_l - N_p I_{os}\left(\mathrm{e}^{\alpha\left(\frac{v_{pv}}{N_s}+\frac{R_s i_{pv}}{N_p}\right)} - 1\right) - \frac{N_p}{R_{sh}}\left(\frac{v_{pv}}{N_s}+\frac{R_s i_{pv}}{N_p}\right) \tag{13}$$

where, N_P is the number of parallel strings, I_l is the light generated current (A), I_{os} is the reverse saturation current (A), v_{pv} is the PV module output voltage (V), i_{pv}

is the PV module output current (A), I_{pv} is the PV array output current (A), N_s is the number of modules connected in series, R_s is the module series resistance and R_{sh} is the module shunt resistance.

Figure 2 shows the MATLAB/Simulink implementation of the designed PV/battery-powered CP system.

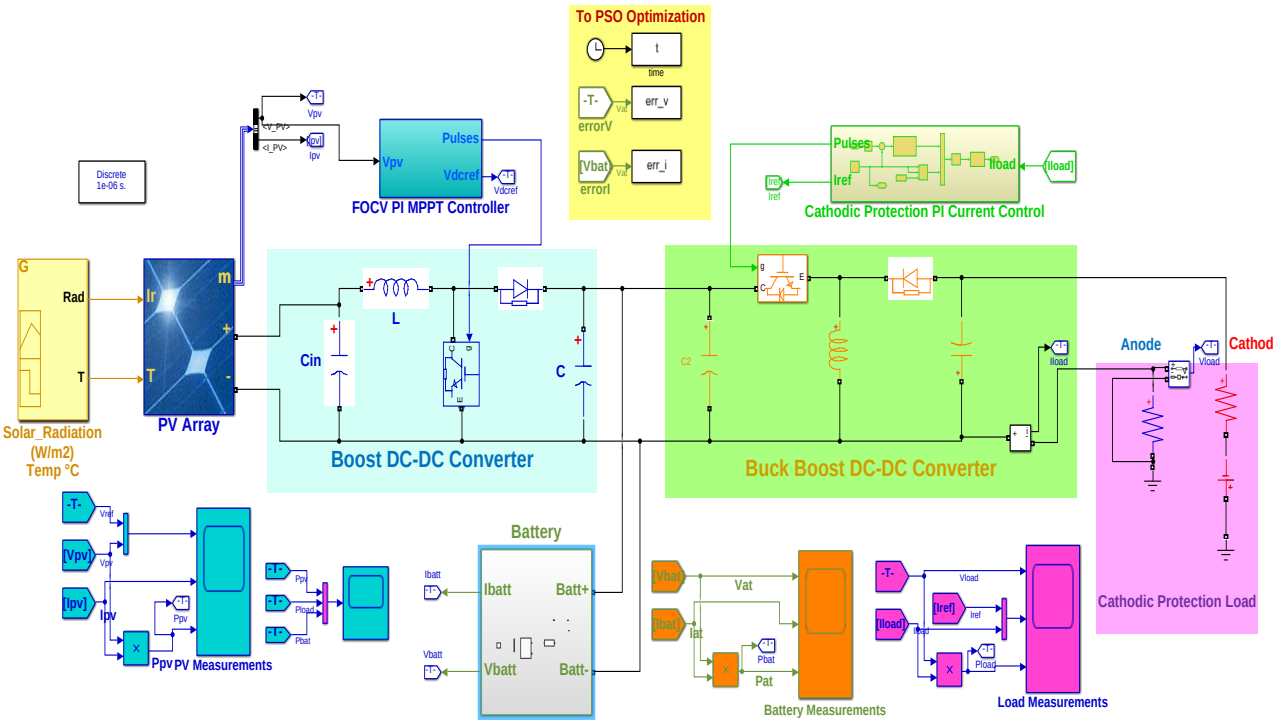

Figure 2. MATLAB/Simulink model of the stand-alone PV-powered CP system.

3.1. Boost Converter Control

As it is clarified previously the main function of the boost DC-DC converter, which steps up the input PV voltage, is to extract the PV array MPP and to transfer it to the CP load or to the system battery. Thus, the control scheme of this converter has to perform this task. The FOCV method is a well-known MPPT algorithm, which is well-suited for low-power applications due to its good performance and low power consumption, is designed in this work and used to continuously estimate the desired PV array MPP voltage, V_{mpp}^{*}, based on detecting the open-circuit voltage, V_{oc}, of the PV array, as [26]:

$$V_{mpp}^{*} = k_v \times V_{oc} \tag{14}$$

where k_v is a characteristic fraction for the considered PV array, which is assumed to remain relatively constant for all radiation levels. The FOCV algorithm periodically samples the V_{oc} to linearly estimate V_{mpp}^{*}. It then forces the PV array to operate at the estimated V_{mpp}^{*} using PI controller, as shown in Figure 3. Where, the error signal, which is the difference between V_{mpp}^{*} and the actual PV voltage is utilized by the PI controller to yield the boost converter duty cycle, D, that can

adjust the input characterizes of the converter to continuously match the ideal PV characteristics. Therefore, this allows the PV array to operate continuously at the MPP whatever the value of the incident solar radiation.

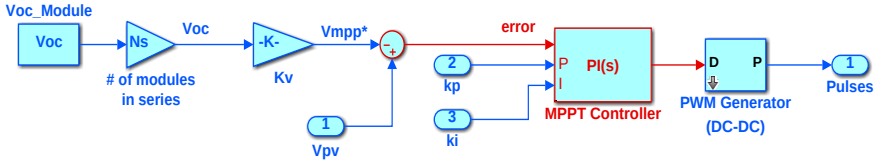

Figure 3. Control block diagram of the boost converter.

3.2. Battery Regulator and Dump Load Control

In this work, the battery regulator is designed as a bidirectional switch, configured with two anti-parallel or inverse-parallel switches (e.g., two IGBTs). These switches can pass currents in reverse directions. They are controlled using separate two ON-OFF control signals, such that the two switches cannot be ON at the same time. One switch charges the battery, while the other discharges it. The control of both switches is achieved using a relay with hysteresis to prevent relay switch-over issues that could ultimately damage the utilized main switches. The main function of this regulator is to safely charge and discharge the system battery and, at the same time, coordinate the control of power flow within the CP system. The control strategy that is designed for the battery regulator and the dump load is indicated in Table 3. As shown this strategy is based on the IF-THEN rules;

Table 3. Control strategy of the battery regulator and the dump load.

Operating Condition	Charge Switch	Discharge Switch	Dump Load Switch	Case of CP Load
$(P_{PV} > P_L^*)$ & $(V_{Bmin} \le V_B < V_{Bmax})$	ON	OFF	OFF	Satisfied from PV only
$(P_{PV} > P_L^*)$ & $(V_B \ge V_{Bmax})$	OFF	OFF	ON	Satisfied from PV only
$(P_{PV} > P_L^*)$ & $(V_B \le V_{Bmin})$	ON	OFF	OFF	Satisfied from PV only
$(P_{PV} < P_L^*)$ & $(V_{Bmin} < V_B \le V_{Bmax})$	OFF	ON	OFF	Satisfied from PV and battery
$(P_{PV} < P_L^*)$ & $(V_B \ge V_{Bmax})$	OFF	ON	OFF	Satisfied from PV and battery
$(P_{PV} < P_L^*)$ & $(V_B \le V_{Bmin})$	OFF	OFF	OFF	Partially satisfied using PV only
$(P_{PV} = P_L^*)$	OFF	OFF	OFF	Satisfied from PV only

such that the IF-part of a rule represents the current situation of the CP system, while the THEN-part represents the suitable ON/OFF switching control signals of

the battery charging and discharging switches and also the suitable ON/OFF switching control signal that can activate or deactivate the dump load. It is indicated that the dump load will be active in only one case, *i.e.*, when the available PV power, PPV, is greater than the desired CP load power, P_L^*, and, at the same time, the system battery is fully charged. Also, the battery will be charged in two cases, *i.e.*, when there is an excess in PV power and its state of charge, SOC, which is measured in this work in terms of the battery voltage, VB, indicates that the battery is fully or partially discharge. Moreover, the battery will be discharged in two cases as well, *i.e.*, when there is a deficit in the available PV power and its *SOC* indicates that the battery is fully or partially charged. Noting that V_{Bmax} is used to express the end of charge voltage of the battery or its maximum permissible *SOC*, and V_{Bmin} is used to express the end of discharge voltage of the battery or its maximum permissible DOD.

3.3. Buck-Boost Converter Control

It is known that the main function of the buck-boost DC-DC converter utilized in this work is to continuously provide the CP load with the constant current needed to perform the CP of the pipeline. Therefore, the designed control scheme of this converter has to achieve this task properly, as indicated in **Figure 4**. It is suggested that the error signal, in this case, which is the difference between the desired CP load current and the actual one, is utilized by the PI controller to yield the control signal needed to control the duty cycle of the buck-boost converter, which can in turn step-up or step-down the converter's output voltage to the value that can continuously regulate the CP load current according to the available input DC link power.

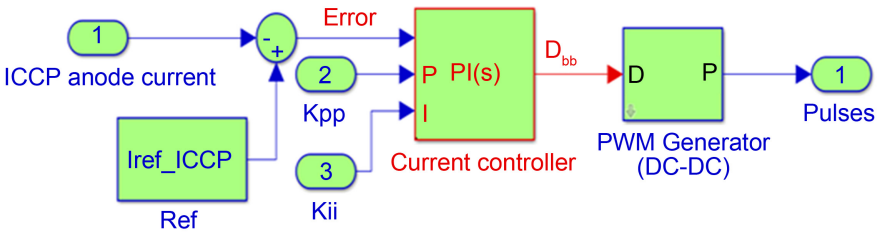

Figure 4. Control block diagram of the buck-boost converter.

3.4. PI Controllers Optimization Using PSO

PSO was initially presented by Kennedy and Eberhart [27] [28] as a nature-inspired metaheuristic algorithm. This method is derived from the social behavior of flocking birds. In PSO, each potential solution, referred to as a "particle," navigates through the problem's search space. The collection of these candidate solutions is known as the particle swarm. During a given iteration k, the i^{th} particle is characterized by its position vector, X_i^k and velocity vector v_i^k in the search space. The fitness of each particle position is determined by the value of the fitness/objective function being optimized. The best previous position encountered by

particle i is stored as $pbest_i$. The best position found by all particles thus far is denoted as *gbest*. The particles modify their flight velocities based on their own experiences and neighboring particles' successes. The behavior of the particles is represented by the following equations [28]:

$$v_i^{k+1} = wv_i^k + c_1 rand_{1i}\left(pbest_i - X_i^k\right) + c_2 rand_{2i}\left(gbest - X_i^k\right) \tag{15}$$

$$X_i^{k+1} = X_i^k + v_i^{k+1} \tag{16}$$

where, v_i^{k+1} is the particle's i updated velocity, X_i^{k+1} is the particle's i updated position at iteration $k+1$, w is the weight inertia, c_1, c_2 are positive acceleration constants, while $rand_{1i}$, $rand_{2i}$ are random numbers [0 and 1]. The optimization continues until the stopping condition is satisfied, which occurs when the predetermined maximum number of iterations is reached.

The two PI controllers' proportional (K_P, K_{pp}) and integral (K_I, K_{ii}) gains for FOCV-based MPPT and current control are optimized using the PSO algorithm. The main objective is to minimize the error, which is calculated according to the integral time absolute error (ITAE) formula [25], as shown in Equation (17). **Figure 5** represents the flowchart of the optimization methodology of the PI gains.

$$\text{fitness function, } f\left(K_p, K_i\right) = \min . \int_0^t \left| error\left(V_{pv}(t)\right)\right| \times t dt \tag{17}$$

$$\text{fitness function, } f\left(K_{pp}, K_{ii}\right) = \min . \int_0^t \left| error\left(I_{iccp}(t)\right)\right| \times t dt \tag{18}$$

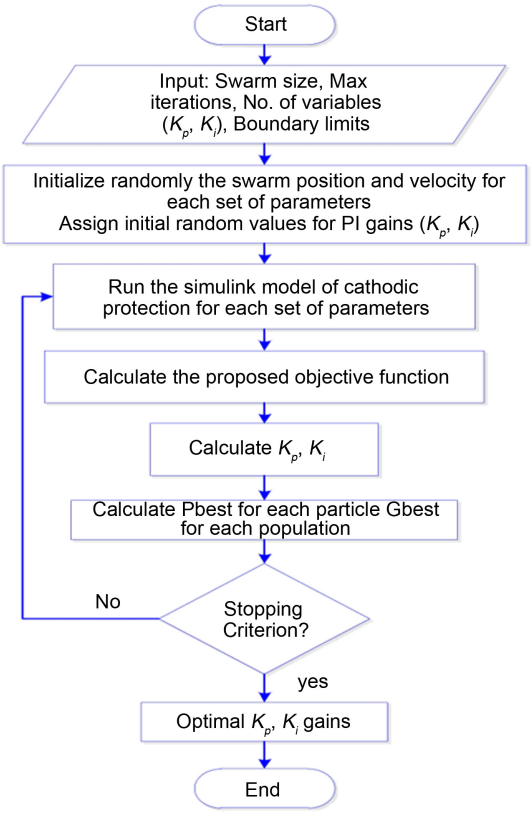

Figure 5. Flowchart of PSO for PI controller optimization.

4. Results and Discussion

This section is dedicated to exhibiting and exploring the obtained simulation results of the designed CP system. The utilized parameters of the designed DC-DC converters of the CP system are indicated in Table 4. Table 5 illustrates the optimized PI gains of the two designed PI controllers using the PSO optimization algorithm.

Table 4. Design parameters of DC-DC converters of the CP system.

Design Parameter	Boost Converter	Buck-Boost Converter
Inductance (L)	370 μH	220 μH
Capacitance (C)	880 μF	2400 μF
Input voltage (V_{in})	30 V	48 V
Output voltage (V_{out})	48 V	44.5 V
Switching frequency (f_s)	5 kHz	5 kHz
Maximum output current (I_{max})	18.3 A	5.745 A

Table 5. Optimized PI gains using PSO.

Optimized PI Gains	PI-FOCV-MPPT controller	ICCP-PI current controller
K_p, K_{pp}	0.7067	0.0209
K_i, K_{ii}	145.4924	201.9398

In this study, the Aavid Solar ASMS-220P module was selected. It provides 220 watts of nominal maximum power, arranged as 1 series module and 4 parallel strings, to represent the PV array. The verification of the PV array is illustrated in Figure 6, showcasing the I-V and P-V characteristics of the specified PV array using MATLAB. In this study, the battery bank is modeled using MATLAB's built-in battery model, which employs a generic dynamic framework that can represent the most widely used types of rechargeable batteries. Figure 7 displays the validation results for the dynamic battery model in MATLAB, featuring the discharge curves of the 100 Ah, 12 V lead-acid battery model utilized in this simulation.

4.1. PI Optimization for MPPT

Figure 8 illustrates the performance of the MPPT controller in regulating the photovoltaic array output voltage under varying solar irradiance conditions. The simulated MPPT utilizes the optimized FOCV algorithm to continuously monitor the PV characteristics and maintain the optimal operating voltage. In the step response testing, the solar irradiance level is manually altered between low, medium, and high-intensity values. This change creates fast transitions that stimulate the MPPT controller. As shown, when irradiance increases sharply from 100 W/m^2 to 1000 W/m^2, the MPPT promptly acts to stabilize the PV voltage at the

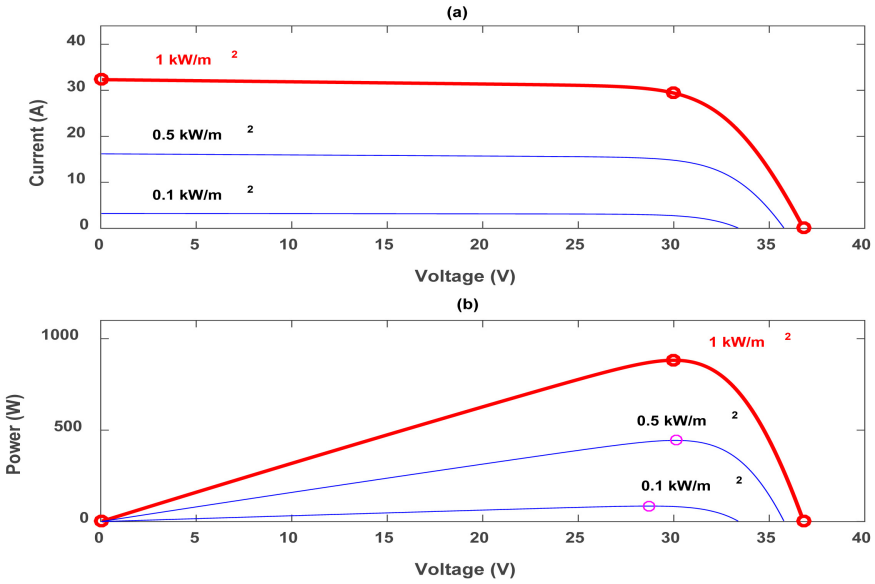

Figure 6. Characteristics of PV array at different radiation levels: (a) I-V characteristics, (b) P-V characteristics.

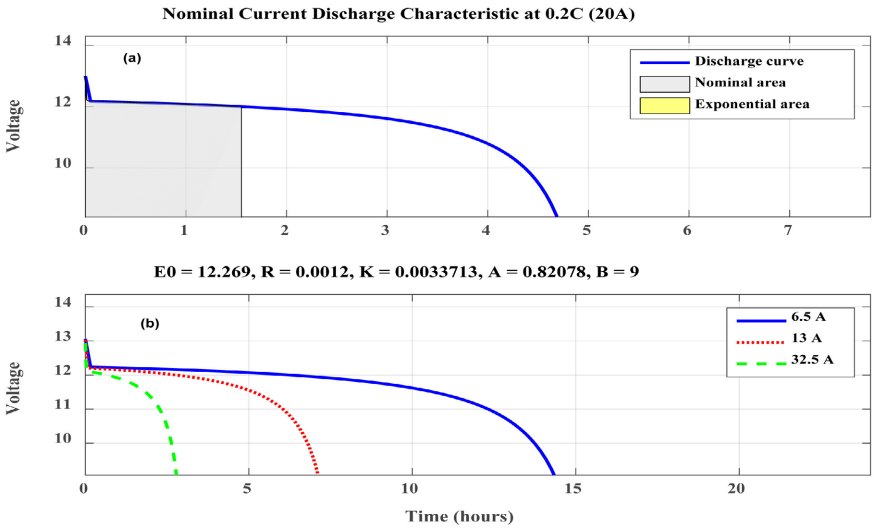

Figure 7. Battery discharge curve: (a) at nominal discharge current, (b) at specified discharge currents.

predetermined set point of 30 V. Similarly, during a fast decrease in irradiance from 1000 W/m^2 to 100 W/m^2, the controller effectiveness holds the voltage steady.

Moreover, during the transition from 500 W/m^2 to 1000 W/m^2 and decreases from 1000 W/m^2 to 500 W/m^2, the MPPT also drives the PV array to its MPP voltage of 30 V. The ability of the FOCV MPPT to instantaneously detect changes and drive the PV array to its MPP voltage, regardless of the irradiation magnitude or rate of fluctuation, is demonstrated. Once each irradiation transition occurs, the PV voltage settles quickly at the optimal 30 V level and remains fixed until the next simulated disturbance. The results confirm that the MPPT implementation

precisely fulfills its role in extracting the maximum available power from the solar modules under all dynamic radiation conditions.

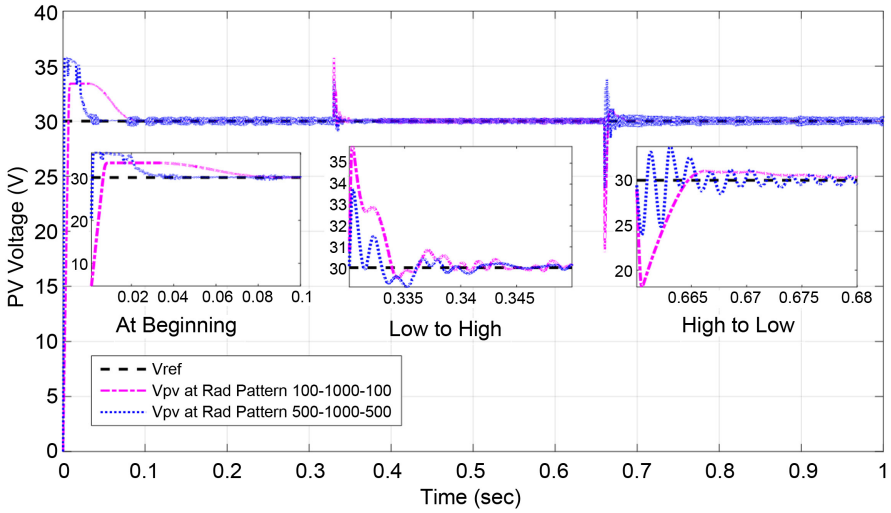

Figure 8. MPPT FOCV-PI controller: PV voltage.

4.2. PI Optimization for ICCP Current Control

Figure 9 illustrates the performance of the optimized PI current controller in regulating the CP anode bed load. The controller aims to maintain a constant current of 5.745 A to the anode. Under varying solar irradiance conditions, step changes are simulated between high and low radiation levels, which assess the controller's response to fast transitions. When solar intensity increases sharply from low to high irradiance, the PI controller immediately operates the buck-boost converter duty cycle to stabilize the anode current at the 5.745 A set point. Similarly, during a quick decrease from high to low irradiance, the controller effectively returns the current to its reference value. This confirms that the controller fulfills its role in accurately maintaining the protective current for CP underground pipelines by precisely regulating the anode bed, even under rapidly changing solar conditions. The PI parameters were optimized during design to achieve this precise and stable control performance.

Figure 10 presents results for two simulation days: sunny and cloudy: showing the daily solar irradiance, PV voltage (V_{pv}), PV current, and duty cycle output from the MPPT controller. The PV voltage stabilizes around 30 V consistently, confirming that the proposed FOCV MPPT algorithm successfully tracks the reference voltage, V_{mpp}^{*}, at the converter output. Variations in the PV output current closely follow the pattern of the solar irradiance levels, demonstrating the strong correlation between incident radiation and photocurrent generation. The duty cycle is seen to vary dynamically in response to changes in solar irradiance over each day from sunrise to sunset. This modulation of the boost converter duty cycle by the MPPT controller ensures regulation of the PV operating point at the MPP for maximum power harvesting under all irradiation conditions.

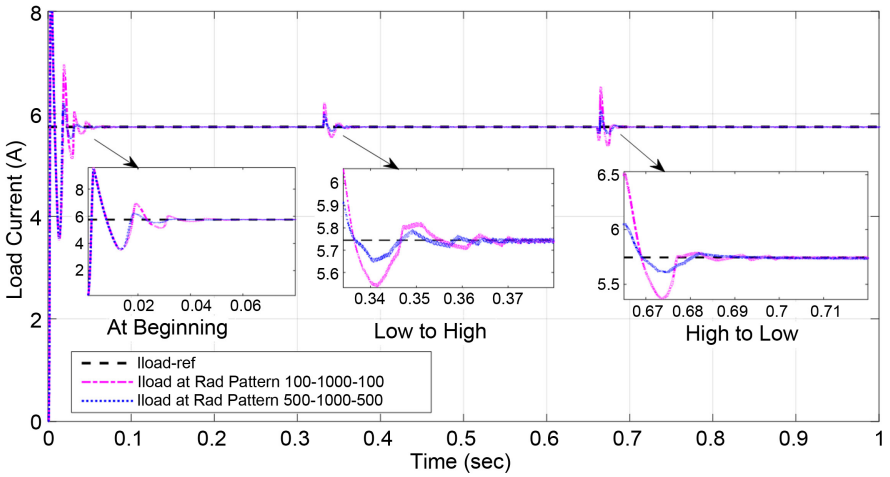

Figure 9. Cathodic protection PI controller anode current.

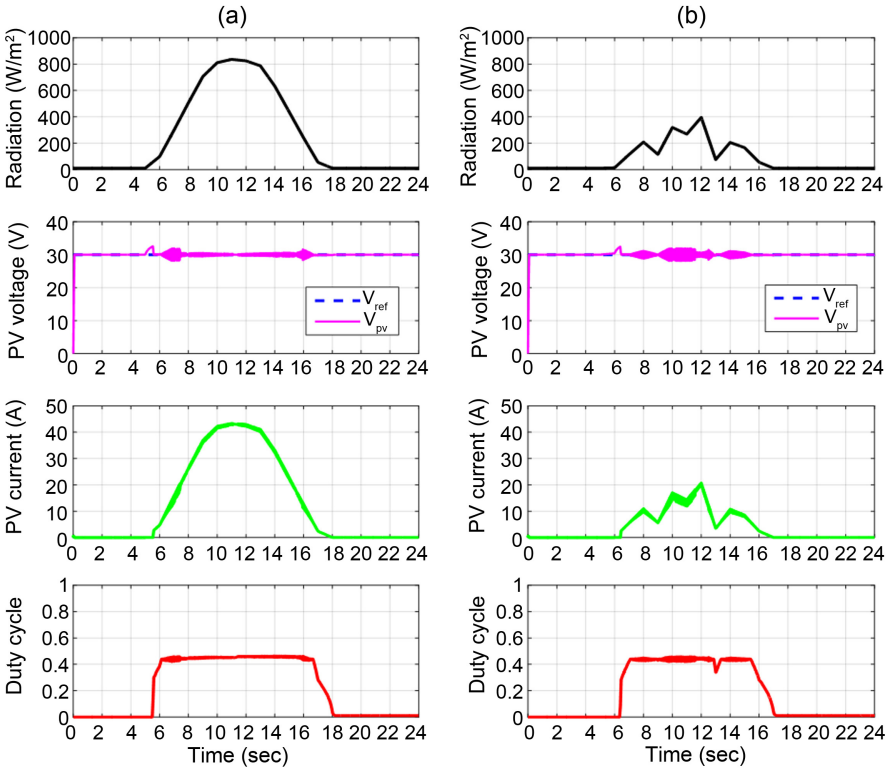

Figure 10. PV array output at (a) sunny day, (b) cloudy day.

These results validate the adequate performance of the FOCV MPPT approach in adapting the boost converter regulation to fluctuations in solar input to maintain an optimal 30 V output and maximum power tracking under the wide range of seasonal and daily irradiance variations considered.

Figure 11 shows the results of the battery testing. The variation in battery voltage is much higher during the charging cycle than discharging. However, the voltage remains within acceptable limits for both cycles. The controller monitors solar power input and battery voltage during the charging state. It controls switches

connected to the battery to maintain the charging current and keep the voltage below its maximum safe level. In the discharging state, the controller observes the load demand versus the available solar power. It operates switches connected to the battery to draw current when solar power cannot meet the load demand, as long as the battery's voltage is above the minimum safe level. This testing demonstrates how the control system regulates the charging and discharging of the battery to keep it operating efficiently and within technical specifications.

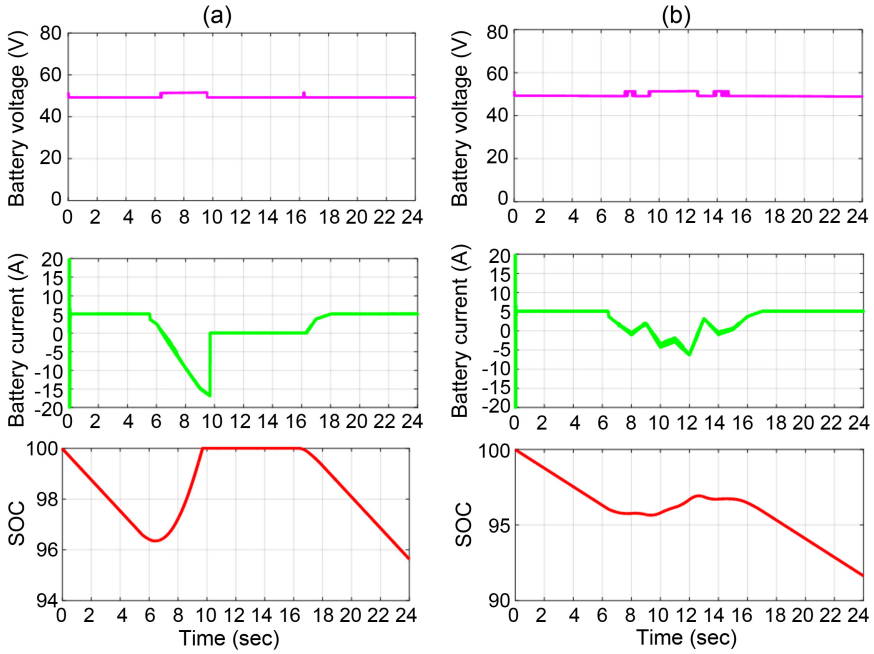

Figure 11. Battery output (a) sunny day, (b) cloudy day.

Figure 12 shows the daily load current and voltage curve distribution for a typical winter and summer day. It also depicts the duty cycle of the converter. The results demonstrate that a constant load voltage of 44 V and a load current of 5.745 A are maintained daily. Additionally, the measured load current closely tracks the reference load current value. This figure illustrates how the system regulates load voltage and current to keep them consistent with the reference values throughout a daily cycle during different seasons. The converter performs well in matching the actual load to the target load level.

Figure 13 shows the waveforms of load power, PV array output Power, and battery output power at different radiation levels. The battery supplements the load with the needed power (discharging mode) at low radiation levels. As the solar radiation level steps up and when the PV output power exceeds the load power, the battery turns on to the charging mode until reaching total capacity (*i.e.*, SOC = 1). In that case, the battery power equals zero (*i.e.* neither charging nor discharging). The waveforms for charging and discharging the battery indicate that when the power from the PV system exceeds the power consumed by the load, the battery begins to charge. In times of low generation, the battery will

supply additional energy to help maintain energy balance.

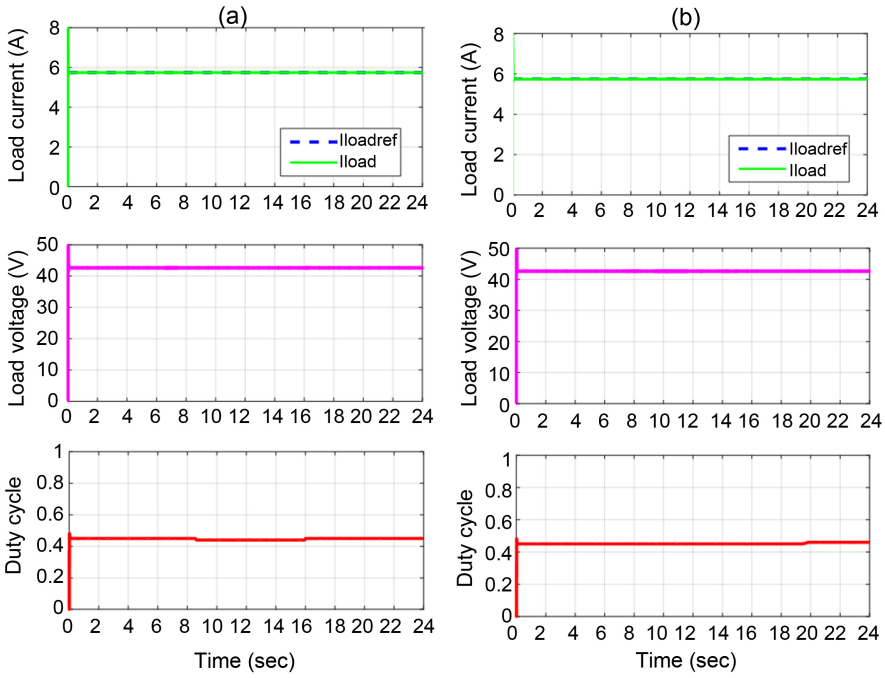

Figure 12. CP load consumption (a) sunny day, (b) cloudy day.

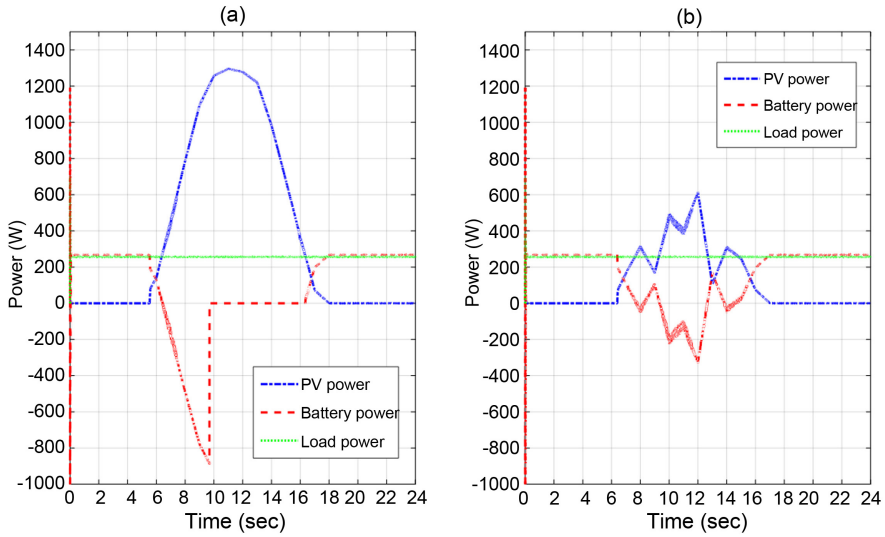

Figure 13. PV power, battery power, load power: (a) sunny day, (b) cloudy day.

5. Conclusions

This paper presented the design, control, and simulation of a standalone PV-powered CP system for underground pipelines. The system aims to continuously supply a constant anode current (5.745 A) required for the ICCP. It comprises a PV array, storage battery, and two DC-DC converters: a boost converter for the MPPT of the PV array and a buck-boost converter to regulate the anode current. A battery regulator ensures safe charging and discharging of the battery. The DC-DC

converters are controlled using optimally tuned PI controllers, with parameters determined by the PSO technique. The system is simulated in MATLAB/Simulink platform to validate its ability to:

- Operate the PV array at maximum power under varying solar radiation.
- Safely manage battery charging and discharging.
- Provide a stable, constant anode current for corrosion protection.

Simulation results demonstrate the system's ability to achieve these objectives. However, real-world implementation and experimental validation remain future steps to confirm the system's feasibility and performance in practical settings.

Conflicts of Interest

The authors declare no conflicts of interest regarding the publication of this paper.

References

[1] Al-Moubaraki, A.H. and Obot, I.B. (2021) Corrosion Challenges in Petroleum Refinery Operations: Sources, Mechanisms, Mitigation, and Future Outlook. *Journal of Saudi Chemical Society*, **25**, Article ID: 101370. https://doi.org/10.1016/j.jscs.2021.101370

[2] Maka, A.O.M., Chaudhary, T.N., Alaswad, G. and Elsayah, O. (2024) Applications of Solar Photovoltaics in Powering Cathodic Protection Systems: A Review. *Clean Technologies and Environmental Policy*, **26**, 2755-2776. https://doi.org/10.1007/s10098-024-02750-0

[3] Alamri, A.H. (2020) Localized Corrosion and Mitigation Approach of Steel Materials Used in Oil and Gas Pipelines—An Overview. *Engineering Failure Analysis*, **116**, Article ID: 104735. https://doi.org/10.1016/j.engfailanal.2020.104735

[4] Carmona, J., Garcés, P. and Climent, M.A. (2015) Efficiency of a Conductive Cement-Based Anodic System for the Application of Cathodic Protection, Cathodic Prevention and Electrochemical Chloride Extraction to Control Corrosion in Reinforced Concrete Structures. *Corrosion Science*, **96**, 102-111. https://doi.org/10.1016/j.corsci.2015.04.012

[5] Ashworth, V. (2010) Principles of Cathodic Protection. In: Richardson, T.J.A., Ed., *Shreir's Corrosion*, Elsevier, 2747-2762. https://doi.org/10.1016/b978-044452787-5.00152-9

[6] Ameh, E.S. and Ikpeseni, S.C. (2018) Pipelines Cathodic Protection Design Methodologies for Impressed Current and Sacrificial Anode Systems. *Nigerian Journal of Technology*, **36**, 1072-1077. https://doi.org/10.4314/njt.v36i4.12

[7] Abdulamer, D. and Abdulamer, D.N. (2013) Effect of Soil Resistivities for Different Geometrical Anodes on Design Photovoltaic for Cathodic Protection System. *Global Research Analysis*, **2**, 36-40. https://www.researchgate.net/publication/348550363

[8] Abdulamer, D.N. (2013) Effect of Soil Resistivity on the Design of Sacrificial Anode Cathodic Protection System. *Journal of Petroleum Research and Studies*, **4**, 142-158. https://doi.org/10.52716/jprs.v4i3.121

[9] Al-Refai, M.A. (2019) Optimal Design and Simulation of Solar Photovoltaic Powered Cathodic Protection for Underground Pipelines in Libya. *Journal of Electrical Engineering*, **7**, 61-74. https://doi.org/10.17265/2328-2223/2019.02.004

[10] Mohammed, S.A.H. and Abdulbaqi, I.M. (2018) Numerical Study and Design of an Impressed Current Cathodic Protection System for Buried Metallic Pipes. 2018 *Third Scientific Conference of Electrical Engineering* (*SCEE*), Baghdad, 19-20 December 2018, 95-100. https://doi.org/10.1109/scee.2018.8684076

[11] Mohammed, S.A.D.H. and Abdulbaqi, I.M. (2020) Design and Implementation of an Impressed Current Cathodic Protection System for Buried Metallic Pipes (Part II) (Considering Al-Quds Gas Station in Baghdad). *International Journal of Power Electronics and Drive Systems* (*IJPEDS*), **11**, 275-293. https://doi.org/10.11591/ijpeds.v11.i1.pp275-283

[12] Khudoyorov, K.D. (2022) Automatic Control of Photovoltaic Cathodic Protection System Used for Various Metals. *Applied Solar Energy*, **58**, 244-249. https://doi.org/10.3103/s0003701x22020098

[13] Javidan, J. (2016) Energy Management Strategy of Stand-Alone Photovoltaic System in Cathodic Protection Pipeline. *Journal of Operation and Automation in Power Engineering*, **4**, 143-152. http://joape.uma.ac.ir

[14] Javadi, M., Javidan, J. and Salimi, M. (2014) Design an Intelligent Solar Photovoltaic Power for Cathodic Protection System to Protect Under Ground Gas Pipeline. *International Journal on Technical and Physical Problems of Engineering*, **18**, 27-33. http://www.iotpe.com

[15] Haddadi, M., Ali, M. and Krishan, M. (2009) Optimized Design of a Photovoltaic Cathodic Protection. *The Arabian Journal for Science and Engineering*, **34**, 477-489. https://www.researchgate.net/publication/228675646

[16] Laoun, B., Niboucha, K. and Serir, L. (2023) Cathodic Protection of a Buried Pipeline by Solar Energy. *Journal of Renewable Energies*, **12**, 99-104. https://doi.org/10.54966/jreen.v12i1.123

[17] Samir Adly, G., Anis, W.R. and Hafez, I.M. (2017) Design of Photovoltaic Powered Cathodic Protection System. *International Journal of Scientific & Technology Research*, **6**, 246-253. https://www.ijstr.org

[18] Sada, B., Ali, R. and Ali, K. (2016) Identification and Control of Impressed Current Cathodic Protection System. *Iraqi Journal for Electrical and Electronic Engineering*, **12**, 214-220. https://doi.org/10.37917/ijeee.12.2.12

[19] Javadi, M., Javidan, J. and Salimi, M. (2014) Cathodic Protection of an Underground Pipeline by Photovoltaic Power System Using Intelligent Method. *International Journal of Renewable Energy Research*, **4**, 267-274.

[20] Akcayol, M.A. (2006) Application of Fuzzy Logic Controlled Cathodic Protection on Iraq-Turkey Crude Oil Pipeline. *Applied Intelligence*, **24**, 43-50. https://doi.org/10.1007/s10489-006-6928-x

[21] Samoudi, A.J.K. (2015) Design and Simulation of Solar Photovoltaic Powered Cathodic Protection Systems. Master Thesis, An-Najah National University.

[22] Nafeh, A.E.A. (2009) Design and Economic Analysis of a Stand-Alone PV System to Electrify a Remote Area Household in Egypt. *The Open Renewable Energy Journal*, **2**, 33-37. https://doi.org/10.2174/1876387100902010033

[23] Zahedi, A. and Kalam, A. (2000) Balancing Cost and Performance in a PV/Wind/Battery Hybrid Power System. 2020 *Australasian Universities Power Engineering Conference* (*AUPEC* 2020), 29 November-3 December 2020, Hobart, 1-5.

[24] Mosalam Shaltout, M.A. (1998) Egyptian Solar Radiation Atlas. New and Renewable Energy Authority, Ministry of Electrical and Energy, Egypt.

[25] Hassan, A.A., Fahmy, F.H., Nafeh, A.E.S.A. and Youssef, H.K.M. (2022) Control of

Three-Phase Inverters for Smart Grid Integration of Photovoltaic Systems. *Journal of Electrical Systems*, **18**, 109-131.

[26] Frezzetti, A., Manfredi, S. and Suardi, A. (2014) Adaptive Focv-Based Control Scheme to Improve the MPP Tracking Performance: An Experimental Validation. *IFAC Proceedings Volumes*, **47**, 4967-4971. https://doi.org/10.3182/20140824-6-za-1003.02464

[27] Eberhart, R. and Kennedy, J. (1995) A New Optimizer Using Particle Swarm Theory. *MHS'*95. *Proceedings of the Sixth International Symposium on Micro Machine and Human Science*, Nagoya, 4-6 October 1995, 39-43. https://doi.org/10.1109/mhs.1995.494215

[28] Gad, A.G. (2022) Particle Swarm Optimization Algorithm and Its Applications: A Systematic Review. *Archives of Computational Methods in Engineering*, **29**, 2531-2561. https://doi.org/10.1007/s11831-021-09694-4